Stimulated Brillouin scattering in nanoscale silicon step-index waveguides: a general framework of selection rules and calculating SBS gain

Wenjun Qiu,[1] Peter T. Rakich,[2] Heedeuk Shin,[2] Hui Dong,[3] Marin Soljačić,[1] and Zheng Wang[3,*]

[1]*Department of Physics, Massachusetts Institute of Technology, Cambridge, MA 02139 USA*
[2]*Department of Applied Physics, Yale University, New Haven, CT 06520 USA*
[3]*Department of Electrical and Computer Engineering, University of Texas at Austin, Austin, TX 78758 USA*
[*]*zheng.wang@austin.utexas.edu*

Abstract: We develop a general framework of evaluating the Stimulated Brillouin Scattering (SBS) gain coefficient in optical waveguides via the overlap integral between optical and elastic eigen-modes. This full-vectorial formulation of SBS coupling rigorously accounts for the effects of both radiation pressure and electrostriction within micro- and nano-scale waveguides. We show that both contributions play a critical role in SBS coupling as modal confinement approaches the sub-wavelength scale. Through analysis of each contribution to the optical force, we show that spatial symmetry of the optical force dictates the selection rules of the excitable elastic modes. By applying this method to a rectangular silicon waveguide, we demonstrate how the optical force distribution and elastic modal profiles jointly determine the magnitude and scaling of SBS gains in both forward and backward SBS processes. We further apply this method to the study of intra- and inter-modal SBS processes, and demonstrate that the coupling between distinct optical modes are necessary to excite elastic modes with all possible symmetries. For example, we show that strong inter-polarization coupling can be achieved between the fundamental TE- and TM-like modes of a suspended silicon waveguide.

OCIS codes: (190.2640) Stimulated scattering, modulation, etc.; (220.4880) Optomechanics; (190.4390) Nonlinear optics, integrated optics; (130.2790) Guided waves.

References and links

1. R. Y. Chiao, C. H. Townes, and B. P. Stoicheff, “Stimulated Brillouin scattering and coherent generation of intense hypersonic waves,” Phys. Rev. Lett. **12**, 592–595 (1964).
2. P. Dainese, P. Russell, N. Joly, J. Knight, G. Wiederhecker, H. Fragnito, V. Laude, and A. Khelif, “Stimulated Brillouin scattering from multi-ghz-guided acoustic phonons in nanostructured photonic crystal fibres,” Nat. Phys. **2**, 388–392 (2006).
3. A. Kobyakov, M. Sauer, and D. Chowdhury, “Stimulated Brillouin scattering in optical fibers,” Adv. Opt. Photonics **2**, 1–59 (2010).
4. M. S. Kang, A. Nazarkin, A. Brenn, and P. S. J. Russell, “Tightly trapped acoustic phonons in photonic crystal fibres as highly nonlinear artificial raman oscillators,” Nat. Phys. **5**, 276–280 (2009).

5. R. Pant, C. G. Poulton, D.-Y. Choi, H. Mcfarlane, S. Hile, E. Li, L. Thevenaz, B. Luther-Davies, S. J. Madden, and B. J. Eggleton, "On-chip stimulated Brillouin scattering," Opt. Express **19**, 8285–8290 (2011).
6. M. Tomes and T. Carmon, "Photonic micro-electromechanical systems vibrating at *x*-band (11-ghz) rates," Phys. Rev. Lett. **102**, 113601 (2009).
7. A. Byrnes, R. Pant, E. Li, D. Choi, C. G. Poulton, S. Fan, S. Madden, B. Luther-Davies, and B. J. Eggleton, "Photonic chip based tunable and reconfigurable narrowband microwave photonic filter using stimulated Brillouin scattering," Opt. Express **20**, 18845–18854 (2012).
8. Z. Yu and S. Fan, "Complete optical isolation created by indirect interband photonic transitions," Nat. Photonics **3**, 91–94 (2009).
9. M. S. Kang, A. Butsch, and P. S. J. Russell, "Reconfigurable light-driven opto-acoustic isolators in photonic crystal fibre," Nat. Photonics **5**, 549–553 (2011).
10. C. G. Poulton, R. Pant, A. Byrnes, S. Fan, M. J. Steel, and B. J. Eggleton, "Design for broadband on-chip isolator using stimulated Brillouin scattering in dispersion-engineered chalcogenide waveguides," Opt. Express **20**, 21235–21246 (2012).
11. Z. Zhu, D. J. Gauthier, and R. W. Boyd, "Stored light in an optical fiber via stimulated Brillouin scattering," Science **318**, 1748–1750 (2007).
12. Y. Okawachi, M. S. Bigelow, J. E. Sharping, Z. Zhu, A. Schweinsberg, D. J. Gauthier, R. W. Boyd, and A. L. Gaeta, "Tunable all-optical delays via Brillouin slow light in an optical fiber," Phys. Rev. Lett. **94**, 153902 (2005).
13. K. Y. Song, M. Herráez, and L. Thévenaz, "Observation of pulse delaying and advancement in optical fibers using stimulated Brillouin scattering," Opt. Express **13**, 82–88 (2005).
14. K. Y. Song, K. S. Abedin, K. Hotate, M. G. Herráez, and L. Thévenaz, "Highly efficient Brillouin slow and fast light using As2Se3 chalcogenide fiber," Opt. Express **14**, 5860–5865 (2006).
15. R. Pant, M. D. Stenner, M. A. Neifeld, and D. J. Gauthier, "Optimal pump profile designs for broadband sbs slow-light systems," Opt. Express **16**, 2764–2777 (2008).
16. R. Pant, A. Byrnes, C. G. Poulton, E. Li, D. Choi, S. Madden, B. Luther-Davies, and B. J. Eggleton, "Photonic-chip-based tunable slow and fast light via stimulated Brillouin scattering," Opt. Lett. **37**, 969–971 (2012).
17. T. Kurashima, T. Horiguchi, and M. Tateda, "Distributed-temperature sensing using stimulated Brillouin scattering in optical silica fibers," Opt. Lett. **15**, 1038–1040 (1990).
18. A. Schliesser, R. Riviere, G. Anetsberger, O Arcizet, and T. J. Kippenberg, "Resolved-sideband cooling of a micromechanical oscillator," Nat. Phys. **4**, 415–419 (2008).
19. G. Bahl, M. Tomes, F. Marquardt, and T. Carmon, "Observation of spontaneous Brillouin cooling," Nat. Phys. **8**, 203–207 (2012).
20. W. C. Jiang, X. Lu, J. Zhang, and Q. Lin "High-frequency silicon optomechanical oscillator with an ultralow threshold," Opt. Express **20**, 15991–15996 (2012).
21. H. O. Hill, B. S. Kawasaki, and D. C. Johnson, "CW Brillouin laser," Appl. Phys. Lett. **28**, 608–609 (1976).
22. I. V. Kabakova, R. Pant, D. Choi, S. Debbarma, B. Luther-Davies, S. J. Madden, and B. J. Eggleton, "Narrow linewidth Brillouin laser based on chalcogenide photonic chip," Opt. Lett. **38**, 3208–3211 (2013).
23. Y. R. Shen, N. Bloembergen, "Theory of stimulated Brillouin and Raman scattering," Phys. Rev. **137**, A1787–A1805 (1965).
24. R. Boyd, *Nonlinear Optics*, 3rd ed. (Academic, 2009).
25. G. Agrawal, *Nonlinear Fiber Optics*, 4th ed. (Academic, 2006).
26. J. Botineau, E. Picholle, and D. Bahloul, "Effective stimulated Brillouin gain in singlemode optical fibres," Electron. Lett. **31**, 2032–2034 (1995).
27. J. Wang, Y. Zhu, R. Zhang, and D. J. Gauthier, "FSBS resonances observed in a standard highly nonlinear fiber," Opt. Express **19**, 5339–5349 (2011).
28. A. H. McCurdy, "Modeling of stimulated Brillouin scattering in optical fibers with arbitrary radial index profile," J. Lightwave Technol. **23**, 3509 (2005).
29. X. Huang and S. Fan, "Complete all-optical silica fiber isolator via stimulated Brillouin scattering," J. Lightwave Technol. **29**, 2267–2275 (2011).
30. M. S. Kang, A. Brenn, and P. S. J. Russell, "All-optical control of gigahertz acoustic resonances by forward stimulated interpolarization scattering in a photonic crystal fiber," Phys. Rev. Lett. **105**, 153901 (2010).
31. P. T. Rakich, C. Reinke, R. Camacho, P. Davids, and Z. Wang, "Giant enhancement of stimulated Brillouin scattering in the subwavelength limit," Phys. Rev. X **2**, 011008 (2012).
32. H. Shin, W. Qiu, R. Jarecki, J. A. Cox, R. H. Olsson III, A. Starbuck, Z. Wang, and P. T. Rakich, "Tailorable stimulated Brillouin scattering in nanoscale silicon waveguides," Nat. Commun. **4**, 1944 (2013).
33. R. Van Laer, D. Van Thourhout, and R. Baets, "Strong stimulated Brillouin scattering in an on-chip silicon slot waveguide," in *CLEO: Science and Innovations*, San Jose, CA, 9–14 June 2013 .
34. P. T. Rakich, M. A. Popovi, M. Soljacic, and E. P. Ippen, "Trapping, corralling and spectral bonding of optical resonances through optically induced potentials," Nat. Photonics **1**, 658–665 (2007).
35. M. Eichenfield, C. P. Michael, R. Perahia, and O. Painter, "Actuation of micro-optomechanical systems via cavity-enhanced optical dipole forces," Nat. Photonics **1**, 416–422 (2007).
36. T. J. Kippenberg and K. J. Vahala, "Cavity optomechanics: Back-action at the mesoscale," Science **321**, 1172–

#197459 - $15.00 USD Received 12 Sep 2013; revised 18 Nov 2013; accepted 18 Nov 2013; published 12 Dec 2013

1176 (2008).
37. M. Eichenfield, J. Chan, R. M. Camacho, K. J. Vahala, and O. Painter, "Optomechanical crystals," Nature **462**, 78–82 (2009).
38. G. S. Wiederhecker, L. Chen, A. Gondarenko, and M. Lipson, "Controlling photonic structures using optical forces," Nature **462**, 633–636 (2009).
39. M. Eichenfield, J. Chan, A. H. Safavi-Naeini, K. J. Vahala, and O. Painter, "Modeling dispersive coupling and-losses of localized optical andmechanical modes in optomechanicalcrystals," Opt. Express **17**, 20078–20098 (2009).
40. M. Li, W. H. P. Pernice, and H. X. Tang, "Tunable bipolar optical interactions between guided lightwaves," Nat. Photonics **3**, 464–468 (2009).
41. J. Roels, I. D. Vlaminck, L. Lagae, B. Maes, D. V. Thourhout, and R. Baets, "Tunable optical forces between nanophotonic waveguides," Nat. Nanotechnol. **4**, 510–513 (2009).
42. Q. Lin, J. Rosenberg, D. Chang, R. Camacho, M. Eichenfield, K. J. Vahala, and O. Painter, "Coherent mixing of mechanical excitations in nano-optomechanical structures," Nat. Photonics **4**, 236–242 (2010).
43. D. Royer and E. Dieulesaint, *Elastic Waves in Solids I: Free and Guided Propagation* (Springer, 2000).
44. Z. Yu and S. Fan, "Complete optical isolation created by indirect interband photonic transitions," Nat. Photonics **3**, 91–94 (2008).
45. P. T. Rakich, P. Davids, and Z. Wang, "Tailoring optical forces in waveguides through radiation pressure and electrostrictive forces," Opt. Express **18**, 14439–14453 (2010).
46. M. L. Povinelli, M. Loncar, M. Ibanescu, E. J. Smythe, S. G. Johnson, F. Capasso, and J. D. Joannopoulos, "Evanescent-wave bonding between optical waveguides," Opt. Lett. **30**, 3042–3044 (2005).
47. P. T. Rakich, Z. Wang, and P. Davids, "Scaling of optical forces in dielectric waveguides: rigorous connection between radiation pressure and dispersion," Opt. Lett. **36**, 217–219 (2011).
48. W. Qiu, P. Rakich, M. Soljacic, and Z. Wang, "Stimulated Brillouin scattering in slow light waveguides," arXiv1210.0738 (2012).
49. S. Chandorkar, M. Agarwal, R. Melamud, R. Candler, K. Goodson, and T. Kenny, "Limits of quality factor in bulk-mode micromechanical resonators," in *IEEE 21st International Conference on Micro Electro Mechanical Systems, 2008. MEMS 2008* (2008), pp. 74–77.
50. E. Dieulesaint and D. Royer, *Elastic Wvaes in Solids II: Generation, Acousto-Optic Interaction, Applications* (Springer, 2000).
51. J. P. Gordon, "Radiation forces and momenta in dielectric media," Phys. Rev. A **8**, 14–21 (1973).
52. P. W. Milonni and R. W. Boyd, "Momentum of light in a dielectric medium," Adv. Opt. Photonics, **2**, 519–553 (2010).
53. S. G. Johnson, M. Ibanescu, M. A. Skorobogatiy, O. Weisberg, J. D. Joannopoulos, and Y. Fink, "Perturbation theory for Maxwell's equations with shifting material boundaries," Phys. Rev. E **65**, 066611 (2002).
54. M. A. Hopcroft, W. D. Nix, and T. W. Kenny, "What is the Youngs Modulus of silicon?," J. Microelectromech. Syst. **19**, 229–238 (2010).
55. L. S. Hounsome, R. Jones, M. J. Shaw, and P. R. Briddon, "Photoelastic constants in diamond and silicon," Phys. Status Solidi A **203**, 3088–3093 (2006).
56. R. Shelby, M. Levenson, and P. Bayer, "Guided acoustic-wave Brillouin scattering," Phys. Rev. B **31**, 5244–5252 (1985).
57. R. Shelby, M. Levenson, and P. Bayer, "Resolved forward Brillouin scattering in optical fibers," Phys. Rev. Lett. **54**, 939-942 (1985).
58. R. Pant, A. Byrnes, C. G. Poulton, E. Li, D.-Y. Choi, S. Madden, B. Luther-Davies, and B. J. Eggleton, "Photonic-chip-based tunable slow and fast light via stimulated Brillouin scattering," Opt. Lett. **37**, 969–971 (2012).
59. A. Byrnes, R. Pant, E. Li, D.-Y. Choi, C. G. Poulton, S. Fan, S. Madden, B. Luther-Davies, and B. J. Eggleton, "Photonic chip based tunable and reconfigurable narrowband microwave photonic filter using stimulated Brillouin scattering," Opt. Express **20**, 18836–18845 (2012).
60. J. Li, H. Lee, T. Chen, and K. J. Vahala, "Characterization of a high coherence, Brillouin microcavity laser on silicon," Opt. Express **20**, 20170–20180 (2012).

1. Introduction

Stimulated Brillouin Scattering (SBS) is a third-order nonlinear process that produces efficient coupling between traveling-wave photons and phonons [1, 2]. Nonlinear coupling through SBS has been widely studied, yielding applications such as optical frequency conversion [3–5], radio frequency signal processing [6, 7], optical isolators [8–10] stopped light [11], slow light [12–16], distributed temperature sensing [17], cooling [18, 19], oscillator [20], and novel lasers sources [21, 22]. Brillouin nonlinearities, which are known to be among the strongest nonlinearities in optical fibers, also show promise as the basis for a number of chip-scale signal pro-

#197459 - $15.00 USD Received 12 Sep 2013; revised 18 Nov 2013; accepted 18 Nov 2013; published 12 Dec 2013

cessing applications through the use of highly nonlinear chalcogenide waveguides [5, 7, 10, 16]. At a basic level, the versatility of Brillouin processes springs from our ability to understand and manipulate this powerful form of photon-phonon coupling in a large variety of waveguide systems.

Over the past several decades, various conceptually simple and useful methods have been employed to predict the strength of SBS coupling within guided-wave systems based on modal overlap integrals [4, 9, 23–30]. Through these treatments, which have proven remarkably accurate for the prediction of SBS in microscale waveguides and fibers, one is often able view Brillouin coupling as arising from intrinsic (or bulk) material nonlinearities. Note that the bulk Brillouin nonlinearity is conventionally defined by a combination of the dispersive, mechanical, and photoelastic properties of a given nonlinear medium [23–25]. This leads to the simple and intuitive notion that Brillouin nonlinearities may be viewed as an intrinsic third-order nonlinearity, akin to Raman and electronic nonlinearities. Within this paradigm, one expects SBS coupling to scale inversely with waveguide modal area, yielding higher nonlinearities as waveguide dimensions are reduced. This paradigm works remarkably well in predicting SBS nonlinearities in a wide variety of fiber and waveguide systems. However, these conventional notions of Brillouin coupling (as a bulk material nonlinearity) fail to predict SBS coupling within nanophotonic silicon waveguides. Despite the radical enhancement of both Raman and electronic nonlinearities in silicon nanophotonics, stimulated Brillouin scattering has entirely eluded observation in silicon waveguides for over a decade, due to the more complex nature of phonon confinement and photon-phonon coupling within nanoscale silicon waveguides [31].

Only recently, with the realization of hybrid photonic-phononic waveguides, has it been possible to demonstrate radically enhanced and engineerable forms of stimulated Brillouin scattering in silicon nanophotonics [32]. Within such nanoscale silicon waveguides, strong light-boundary interactions were found to have a significant impact on photon-phonon coupling. For example, sub-wavelength confinement within high-index-contrast silicon waveguides give rise to new radiation pressure mediated forms of SBS [31–33]. Moreover, elastic wave displacements at the discontinuous boundaries of high-index-contrast waveguides also give rise to nonlinear polarization-currents that yield significant contribution to the overall Brillouin nonlinearity [31]. These new contributions to SBS coupling require a treatment that accurately captures the full-vectorial nature of these boundary interactions [31], and accounts for the emergence of strong radiation pressure induced couplings, which have been shown to play a crucial role in the dynamics of a range of recent nano-optomechanical systems [34–42].

In this article, we present a general method of calculating SBS gain that accurately captures these physics of SBS coupling due to electrostriction and boundary induced radiation pressures in nanoscale silicon photonics. More generally, this method is applicable to the study of Brillouin nonlinearities in any system consisting of transparent dielectric media with any characteristic length-scale. Through this treatment, we develop the general form of the optical force distributions produced by the two interacting optical eigen-modes (e.g. pump and Stokes modes) and the elastic eigen-modes which mediate photon-phonon coupling. Most previous formulations of SBS treat the optical modes as *linearly* polarized and often simplify the elastic mode as a *scalar* density wave. However, we show that the vector nature and the nontrivial spatial distribution of both optical and elastic eigenmodes have to be fully considered. In what follows, the time dependent forms of the electrostrictive and radiation pressure induced forces are used to formulate analytical expressions for the overall Brillouin gain via an overlap integral with the guided elastic-wave eigenmodes. Full-vectorial formulations of the elastic and electromagnetic fields allow the use of the most general form of dielectric and elastic tensors, necessary to treat complex nanophotonic systems in this paper. Both forward-SBS (FSBS) and backward-SBS (BSBS) geometries are explicitly treated, and both intra-modal and inter-modal coupling examples are given in what follows.

Throughout this paper, we refer to radiation pressure induced forces as those derived from the Maxwell stress-tensor (or resulting from the scattering or reflection of light off of boundaries). Whereas electrostrictive forces are defined as those resulting from the coupling of electromagnetic energy to strain degrees of freedom through nonzero photoelastic constants. We show that the boundary induced nonlinearities, derived from these two effects, can dominate as the mode is confined to subwavelength- or nano-scales. With such confinement, boundary interactions (or boundary induced nonlinearities) have a larger role to play than in microscale waveguides due to the large fields produced at the nanoscale boundaries of high-index contrast waveguide systems.

Armed with this formalism, we study the SBS process in a silicon rectangular waveguide. We show that the optical forces responsible for driving FSBS processes are almost entirely transverse. The constructive combination of electrostrictive forces and radiation pressure occurs for certain elastic modes with matching symmetries, and results in large FSBS gain. In contrast, the electrostrictive optical forces in the BSBS configuration are largely longitudinal, yielding nontrivial interference between radiation pressure and electrostrictive couplings as a function of waveguide dimension. Additionally, we show that this formulation of SBS converges perfectly with conventional scalar SBS theories in the plane-wave limit. We further apply this formalism to the study of inter-modal SBS processes involving inter-polarization coupling between TE-like and TM-like modes of a silicon waveguide. Moreover, we show that by coupling optical modes with distinct spatial symmetries, optical forces with a variety of possible symmetries can be generated. These new degrees of freedom offer great flexibility, enabling the generation of elastic modes with a wide range of spatial symmetries, and new forms of Brillouin coupling.

It should be noted that the existence of reflecting material boundaries within a waveguide system can result in hybridization between transverse and longitudinal elastic waves [43]. This elastic-mode hybridization can produce coupling to a large number of complicated eigenmodes with disparate spatial profiles through Brillouin interactions. The following theoretical framework offers a powerful and simple way to link the excitations of individual elastic mode with the properties of pump and Stokes waves. On one hand, this framework elucidates the contributions from individual elastic modes to the overall SBS gain coefficient. This allows for straightforward conceptualization and design of traveling-wave structures that deliberately enhance or suppress SBS for particular elastic modes. On the other hand, this knowledge also enables one to devise optical fields that target the generation of specific phonon modes, when considered in the context of efficient transduction of coherent signals between optical and acoustic domains.

2. Calculating the SBS gain via overlap integral

The interference between pump and Stokes waves generates a time-varying and spatially-dependent optical force distribution that drives excitation of Brillouin active phonons. On resonance, the optical force is simultaneously frequency-matched and phase-matched to an elastic mode, resulting in strong elastic-wave excitations in the waveguide, and efficient coupling between pump and Stokes-wave photons. We start with a general framework of calculating the SBS gain from the field profiles of both the optical and elastic eigen-modes of a waveguide. The axial direction of the axially invariant waveguide is designated as the x direction. In a typical SBS process, a pump wave $\mathbf{E}_p e^{i(k_p x-\omega_p t)}$ and a Stokes wave $\mathbf{E}_s e^{i(k_s x-\omega_s t)}$ generate traveling optical forces that vary in space with a wavevector $q = k_p - k_s$, and oscillate in time at the beat frequency $\Omega = \omega_p - \omega_s$.

Depending on the launching conditions, SBS can be categorized into forward SBS (FSBS) and backward SBS (BSBS). In FSBS, the pump and Stokes waves are launched in the same direction, generating nearly axially-invariant optical forces, which excite standing-wave-like

#197459 - $15.00 USD Received 12 Sep 2013; revised 18 Nov 2013; accepted 18 Nov 2013; published 12 Dec 2013

elastic modes [4,32]. In BSBS, the pump and Stokes waves propagate along opposite directions, generating axially-varying optical forces, which excite traveling-wave elastic modes. Besides launching the pump and Stokes waves into the same spatial optical mode of the waveguide, SBS can also occur with the pump and Stokes waves in disparate spatial modes, for example, by launching into modes with different polarizations [30]. Such inter-modal SBS are important for optical signal isolation [9, 29, 44] and Brillouin cooling of mechanical devices [19]. These different launching conditions will be individually addressed in the later part of the article.

The optical forces that mediate SBS includes the well-known electrostriction force [19, 45], and radiation pressure whose contribution is only recently recognized [31]. Electrostriction is an intrinsic material nonlinearity, which arises from the tendency of materials to become compressed in regions of high optical intensity. Conventionally, only the electrostriction in the form of a body force is considered as the dominant component [24, 25]. However, the discontinuities in both optical intensities and photoelastic constants generate electrostriction pressure on material boundaries, abundant in nanostructures. Radiation pressure is another boundary nonlinearity, arising from the momentum exchange of light with the material boundaries with discontinuous dielectric constant [46, 47]. Radiation pressure is also radically enhanced in nanoscale structures, exemplified in a wide variety of optomechanics applications [34–42]. In this formalism, by considering the superposition of all three forms of optical forces, not only can the SBS gain coefficient be more accurately evaluated for nanoscale waveguides, one can also take advantage of the coherent interference between these three components, to gain new degree of freedoms of tailoring SBS process.

This total optical force, i. e. the coherent superposition of all three components mentioned above, can excite mechanical vibrations which enable the parametric conversion between pump and Stokes waves. Power transfer between guided pump and Stokes waves along the axis of propagation (x) can be describe by the following relation [24]

$$\frac{dP_s}{dx} = gP_pP_s - \alpha_s P_s. \tag{1}$$

Here, P_p and P_s are the guided power of the pump and Stokes waves, and g is the SBS gain. Through particle flux conservation, SBS gain can be expressed as [31]

$$g(\Omega) = \frac{\omega_s}{2\Omega P_p P_s} Re \left\langle \mathbf{f}, \frac{d\mathbf{u}}{dt} \right\rangle, \tag{2}$$

where $\mathbf{f}$ is the total optical force generated by pump and Stokes waves, and $\mathbf{u}$ describes the elastic deformation of the waveguide induced by $\mathbf{f}$. The inner product between two vector fields is defined as the overlap integral over the waveguide cross-section

$$\langle \mathbf{A}, \mathbf{B} \rangle \triangleq \int \mathbf{A}^* \cdot \mathbf{B} ds. \tag{3}$$

The optical power of a waveguide is given by $P = v_g \langle \mathbf{E}, \varepsilon \mathbf{E} \rangle /2$, where v_g is the optical group velocity. Therefore, we have

$$g(\Omega) = \frac{2\omega_s}{v_{gp} v_{gs}} \frac{Im\langle \mathbf{f}, \mathbf{u} \rangle}{\langle \mathbf{E}_p, \varepsilon \mathbf{E}_p \rangle \langle \mathbf{E}_s, \varepsilon \mathbf{E}_s \rangle}. \tag{4}$$

To further simply Eq. (4), we consider the equation governing the elastic response $\mathbf{u}e^{-i\Omega t}$

#197459 - $15.00 USD Received 12 Sep 2013; revised 18 Nov 2013; accepted 18 Nov 2013; published 12 Dec 2013

under external forces $\mathbf{f}e^{-i\Omega t}$. We begin with the ideal case, neglecting the elastic loss [43]

$$-\rho\Omega^2 u_i = \frac{\partial}{\partial x_j} c_{ijkl} \frac{\partial u_l}{\partial x_k} + f_i. \tag{5}$$

Here ρ is the mass density, and c_{ijkl} is the elastic tensor. c_{ijkl} has two important properties: it is symmetric with respect to the first two and last two indices ($c_{ijkl} = c_{jikl}$, $c_{ijlk} = c_{ijkl}$); the interchange of the first two indices and the last two does not affect the value of c_{ijkl}: $c_{klij} = c_{ijkl}$ [43]. In the absence of a driving force $\mathbf{f}$, the equation above becomes the eigen-equation of elastic waves. Using the symmetry properties of c_{ijkl}, we can show that the operator in the left hand side of the eigen-equation is Hermitian [48]. Therefore, the eigen-mode $\mathbf{u}_m e^{-i\Omega_m t}$ satisfies orthogonality condition

$$\langle \mathbf{u}_m, \rho \mathbf{u}_n \rangle = \delta_{mn} \langle \mathbf{u}_m, \rho \mathbf{u}_m \rangle. \tag{6}$$

When $\mathbf{f}$ is present, $\mathbf{u}$ can be decomposed in terms of eigen-modes $\mathbf{u} = \sum_m b_m \mathbf{u}_m$. Using the orthogonality condition, we have

$$b_m = \frac{\langle \mathbf{u}_m, \mathbf{f} \rangle}{\langle \mathbf{u}_m, \rho \mathbf{u}_m \rangle} \frac{1}{\Omega_m^2 - \Omega^2}. \tag{7}$$

We now consider the more general and practical cases, where elastic loss is present. The commonly encountered elastic loss mechanisms are air damping, thermoelastic dissipation, and clamping losses [49]. The first-order effect of loss can be captured by changing Ω_m to a complex value, $\Omega_m - i\Gamma_m/2$. Assuming quality factor $Q_m = \Omega_m/\Gamma_m$ is well above 1, we have,

$$b_m = \frac{\langle \mathbf{u}_m, \mathbf{f} \rangle}{\langle \mathbf{u}_m, \rho \mathbf{u}_m \rangle} \frac{1}{\Omega_m \Gamma_m} \frac{\Gamma_m/2}{\Omega_m - \Omega - i\Gamma_m/2}. \tag{8}$$

Inserting Eq. (8) into Eq. (4), we can see that the total SBS gain is the sum of SBS gains of individual elastic modes, expressed as

$$g(\Omega) = \sum_m G_m \frac{(\Gamma_m/2)^2}{(\Omega - \Omega_m)^2 + (\Gamma_m/2)^2}. \tag{9}$$

The SBS gain of a single elastic mode has a Lorentzian shape and a peak value of

$$G_m = \frac{2\omega Q_m}{\Omega_m^2 v_{gp} v_{gs}} \frac{|\langle \mathbf{f}, \mathbf{u}_m \rangle|^2}{\langle \mathbf{E}_p, \varepsilon \mathbf{E}_p \rangle \langle \mathbf{E}_s, \varepsilon \mathbf{E}_s \rangle \langle \mathbf{u}_m, \rho \mathbf{u}_m \rangle}. \tag{10}$$

where we have used the fact that $\Omega \ll \omega_p, \omega_s$ and $\omega_p \approx \omega_s = \omega$.

Equation (10) provides a general method to calculate the SBS gain of a waveguide with arbitrary cross-section. For example, with the finite element method, one can numerically calculate the pump and Stokes optical modes at a given ω and the elastic modes at the phase-matching wavevector $q = k_p - k_s$. The SBS of each elastic mode can then be calculated by taking the overlap integral between the derived optical forces and the elastic displacement. Here, body forces are integrated over the waveguide cross-section, while pressures are integrated over the waveguide boundaries. Overall, Eq. (10) shows that the SBS gain is determined by the frequency ratio, the elastic loss factor, the optical group velocities, and the overlap integral between optical forces and elastic eigen-modes. In addition, Eq. (10) provides a convenient way to separate the effects of various optical forces. Specifically, the overlap integral is the linear sum of all

#197459 - $15.00 USD Received 12 Sep 2013; revised 18 Nov 2013; accepted 18 Nov 2013; published 12 Dec 2013

optical forces, which becomes

$$\langle \mathbf{f}, \mathbf{u}_m \rangle = \sum_n \langle \mathbf{f}_n, \mathbf{u}_m \rangle. \tag{11}$$

The amplitudes of individual overlap integrals determine the maximal potential contribution from each form of optical forces, while their relative phases produce the interference effect.

A key step of applying Eq. (10) is to calculate optical forces from pump and Stokes waves. Electrostriction forces are derived from electrostriction tensor, with an instantaneous electrostriction tensor is given by [45]

$$\sigma_{ij} = -\frac{1}{2}\varepsilon_0 n^4 p_{ijkl} E_k E_l. \tag{12}$$

where n is the refractive index, and p_{ijkl} is the photoelastic tensor [50]. In a waveguide system, the total electric field is given by $(\mathbf{E}_p e^{i(k_p x - \omega_p t)} + \mathbf{E}_s e^{i(k_s x - \omega_s t)})/2 + c.c.$ Inserting this expression to Eq. (12), and filtering out the components with frequency Ω, we arrive at the time-harmonic electrostrictive tensor of the form $\sigma_{ij} e^{i(qx-\Omega t)}$, with components

$$\sigma_{ij} = -\frac{1}{4}\varepsilon_0 n^4 p_{ijkl}(E_{pk}E_{sl}^* + E_{pl}E_{sk}^*). \tag{13}$$

Since common materials used in integrated photonics have either cubic crystalline lattice (e.g. silicon) or are isotropic (e.g. silica glass), and most waveguide structures are fabricated to be aligned with the principal axes of the material, we consider the crystal structure of the waveguide material to be symmetric with respect to plane $x = 0$, plane $y = 0$, and plane $z = 0$. Therefore, p_{ijkl} is zero if it contains odd number of a certain component. In the contracted notation, Eq. (13) can be written as

$$\begin{bmatrix} \sigma_{xx} \\ \sigma_{yy} \\ \sigma_{zz} \\ \sigma_{yz} \\ \sigma_{xz} \\ \sigma_{xy} \end{bmatrix} = -\frac{1}{2}\varepsilon_0 n^4 \begin{bmatrix} p_{11} & p_{12} & p_{13} & & & \\ p_{12} & p_{22} & p_{23} & & & \\ p_{13} & p_{23} & p_{33} & & & \\ & & & p_{44} & & \\ & & & & p_{55} & \\ & & & & & p_{66} \end{bmatrix} \begin{bmatrix} E_{px}E_{sx}^* \\ E_{py}E_{sy}^* \\ E_{pz}E_{sz}^* \\ E_{py}E_{sz}^* + E_{pz}E_{sy}^* \\ E_{px}E_{sz}^* + E_{pz}E_{sx}^* \\ E_{px}E_{sy}^* + E_{py}E_{sx}^* \end{bmatrix}. \tag{14}$$

The electrostrictive force is given by the divergence of electrostrictive tensor. In a system consisting of domains of homogeneous materials, electrostrictive forces can exist inside each material (producing an electrostriction body force), and at interfaces where discontinuous stresses are present (yielding an electrostrictive pressure). From the divergence of Eq. (14), the electrostrictive body force becomes $\mathbf{f}^{ES} e^{i(qx-\Omega t)}$, with vector components

$$\begin{aligned} f_x^{ES} &= -iq\sigma_{xx} - \partial_y \sigma_{xy} - \partial_z \sigma_{xz} \\ f_y^{ES} &= -iq\sigma_{xy} - \partial_y \sigma_{yy} - \partial_z \sigma_{yz} \\ f_z^{ES} &= -iq\sigma_{xz} - \partial_y \sigma_{zy} - \partial_z \sigma_{zz}. \end{aligned} \tag{15}$$

Similarly, the electrostrictive pressure on the interface between material 1 and 2 is given by $\mathbf{F}^{ES} e^{i(qx-\Omega t)}$, with components

$$F_i^{ES} = (\sigma_{1ij} - \sigma_{2ij}) n_j. \tag{16}$$

Above, we assume that normal vector n points from material 1 to material 2. With a particular choice of phase, an optical mode of the waveguide, $\mathbf{E} e^{i(kx-\omega t)}$, can be expressed as an imaginary-valued E_x and real-valued E_y, E_z. From Eq. (14), we can see that σ_{xx}, σ_{yy}, σ_{zz}, and

#197459 - $15.00 USD Received 12 Sep 2013; revised 18 Nov 2013; accepted 18 Nov 2013; published 12 Dec 2013

σ_{yz} are real while σ_{xy} and σ_{xz} are imaginary. From Eqs. (15) and (16), we can also see that for both electrostriction body force and electrostriction pressure, the transverse component is real while the longitudinal component is imaginary.

The radiation pressure contribution to the optical force is derived from Maxwell Stress Tensor (MST). For a dielectric system ($\mu = 1$) without free charges ($\rho = 0, J = 0$), radiation pressure is localized where the gradient of ε is nonzero [51–53]. For a heterogeneous system consisting of regions of homogeneous materials, radiation pressure only exists on the interfaces where the gradient of ε is nonzero. Since the magnetic fields are continuous at the dielectric boundary, one can show that only the electric part of MST contributes to radiation pressure in this dielectric system. The electric part of instantaneous MST is

$$T_{ij} = \varepsilon_0 \varepsilon (E_i E_j - \frac{1}{2}\delta_{ij} E^2). \tag{17}$$

The instantaneous pressure on the interface between material 1 and 2 is

$$F_i^{RP} = (T_{2ij} - T_{1ij}) n_j. \tag{18}$$

By decomposing the electric field into its normal and tangential components with respect to the dielectric interface $\mathbf{E} = E_n \mathbf{n} + E_t \mathbf{t}$, and using the boundary condition $\varepsilon_1 E_{1n} = \varepsilon_2 E_{2n} = D_n$ and $E_{1t} = E_{2t} = E_t$, we can show that

$$\mathbf{F}^{RP} = -\frac{1}{2}\varepsilon_0 E_t^2 (\varepsilon_2 - \varepsilon_1)\mathbf{n} + \frac{1}{2}\varepsilon_0^{-1} D_n^2 (\varepsilon_2^{-1} - \varepsilon_1^{-1})\mathbf{n}. \tag{19}$$

Inserting the total electric field $(\mathbf{E}_p e^{i(k_p x - \omega_p t)} + \mathbf{E}_s e^{i(k_s x - \omega_s t)})/2 + c.c$ to the expression above, and filtering out the components with frequency Ω, we have a time-harmonic radiation pressure of the form $\mathbf{F}^{RP} e^{i(qx - \Omega t)}$, where $\mathbf{F}^{RP}$ is of the form

$$\mathbf{F}^{RP} = -\frac{1}{2}\varepsilon_0 E_{pt} E_{st}^* (\varepsilon_2 - \varepsilon_1)\mathbf{n} + \frac{1}{2}\varepsilon_0^{-1} D_{pn} D_{sn}^* (\varepsilon_2^{-1} - \varepsilon_1^{-1})\mathbf{n}. \tag{20}$$

Equation (20) reveals that radiation pressure is always normal to the dielectric interface, pointing from high to low index medium. For axially invariant waveguide, this also means radiation pressure is transverse and real.

Combining Eq. (10) with the calculation of optical forces, we are ready to numerically explore the SBS nonlinearity of nanoscale waveguides. Before that, it is instructive to compare Eq. (10) with the conventional BSBS gain [25]. We can show that Eq. (10) converges to the conventional BSBS gain under the plane-wave approximation for both optical and elastic modes. Specifically, consider the coupling between two counter propagating optical plane-waves through an elastic plane-wave. The optical plane-wave is linearly polarized in y direction. The elastic plane-wave is purely longitudinal traveling at velocity V_L. Under this setup, nonzero optical forces include the longitudinal electrostriction body force, and the transverse components of electrostriction pressure and radiation pressure. In the plane-wave limit, only the longitudinal electrostriction body force contributes nonzero overlap integral. This longitudinal force component reduces to

$$f_x^{ES} = -iq\sigma_{xx} = \frac{1}{2} iq\varepsilon_0 n^4 p_{12} E_y^2. \tag{21}$$

Inserting this expression into Eq. (10), and using the fact that $\Omega = qV_L$ and $q = 2k$, we have an

#197459 - $15.00 USD Received 12 Sep 2013; revised 18 Nov 2013; accepted 18 Nov 2013; published 12 Dec 2013

overall Brillouin gain

$$G_0 = \frac{\omega^2 n^7 p_{12}^2}{c^3 \rho V_L \Gamma} \frac{1}{A}, \tag{22}$$

where A is the cross-sectional area of the waveguide. Note that this result is in perfect agreement with the conventional BSBS computed using widely accepted scalar SBS treatments of gain [25]. For waveguides with transverse dimension much greater than the free-space wavelength of light, the plane-wave approximation is valid, and Eq. (10) converges to G_0. For nanoscale waveguides, Eq. (10) can deviate from G_0 significantly because of the vectorial nature of optical and elastic modes, nontrivial mode profiles, as well as the enhanced boundary nonlinearities.

3. Silicon rectangular waveguide: intra-modal coupling

In this section, we apply the general formalism to study the intramodal SBS process of a silicon waveguide suspended in air (Fig. 1 insert). Intramodal process is concerned with the configuration where the pump and the Stokes waves are launched into the same spatial optical mode of the waveguide. And silicon waveguides are of particular interest, because they can be fabricated from standard SOI platforms. In addition, a suspended silicon waveguide provides tight optical confinement through its large refractive index and nearly perfect elastic confinement through a dramatic impedance mismatch with air. Moreover, since radiation pressure is proportional to the difference of dielectric constants across waveguide boundaries and electrostriction force is quadratic over refractive index, both kinds of optical forces are significantly enhanced in high index contrast structures such as silicon waveguides. Here, we consider a silicon waveguide with a rectangular cross-section of a by $0.9a$. For silicon, we use refractive index $n = 3.5$, an isotropic Young's modulus $E = 170 \times 10^9$ Pa, Poisson's ratio $\nu = 0.28$, and density $\rho = 2329 kg/m^3$. Note that we use a simplified isotropic Young's modulus throughout. However, it is important to note that crystalline silicon has nontrivial elastic tensor [54] that depends on the particular crystal orientation under consideration. These tensor properties can easily be incorporated into elastic-mode simulations to accurately model specific experimental device configurations. For example, see Ref. [32]. In addition, we assume that the [100], [010], and [001] symmetry direction of this crystalline silicon coincide with the x, y, and z axis respectively. Under this orientation, the photo-elastic tensor p_{ijkl} in the contracted notation is $[p_{11}, p_{12}, p_{44}] = [-0.09, 0.017, -0.051]$ [55]. The structure has two symmetry planes $y = 0$ and $z = 0$. Both optical modes and elastic modes are either symmetric or anti-symmetric with respect to these planes.

We categorize the fundamental spatial modes of light in the two polarizations as E_{y11} and E_{z11} (Fig. 1(a)). E_{y11} is even with respect to plane $z = 0$ and odd with respect to plane $y = 0$ with a large E_y component. E_{z11} has the opposite symmetries and slightly higher frequencies. Throughout the study, we assume the pump wavelength at 1.55μm. We use a normalized length scale a, such that the corresponding angular frequency ω is in unit of $2\pi c/a$. Note that a different operational frequency along the optical dispersion relations implies a different a. For intramodal coupling, we assume that pump and Stokes waves come from E_{y11}. Since $\Omega/\omega \approx V_L/c$ is on the order of 10^{-4}, pump and Stokes waves approximately correspond to the same waveguide mode $\mathbf{E}e^{i(kx-\omega t)}$. The induced optical force in intra-modal coupling is always symmetric with respect to both plane $y = 0$ and plane $z = 0$. Therefore, we only need to consider elastic modes with the same spatial symmetry (Fig. 1(b)). Using a finite element solver, we calculate the eigen-mode of the suspended waveguide with free boundary conditions (E-modes). To illustrate the hybrid nature of E-modes, we also calculate purely longitudinal modes (P-modes) and purely transverse modes (S-modes) by forcing $u_{y,z} = 0$ or $u_x = 0$ throughout the waveguide. The dispersion diagram indicates that E-modes are either P-mode like or S-mode like at $q = 0$, but become a hybridized wave with both longitudinal and transverse components at

#197459 - $15.00 USD Received 12 Sep 2013; revised 18 Nov 2013; accepted 18 Nov 2013; published 12 Dec 2013

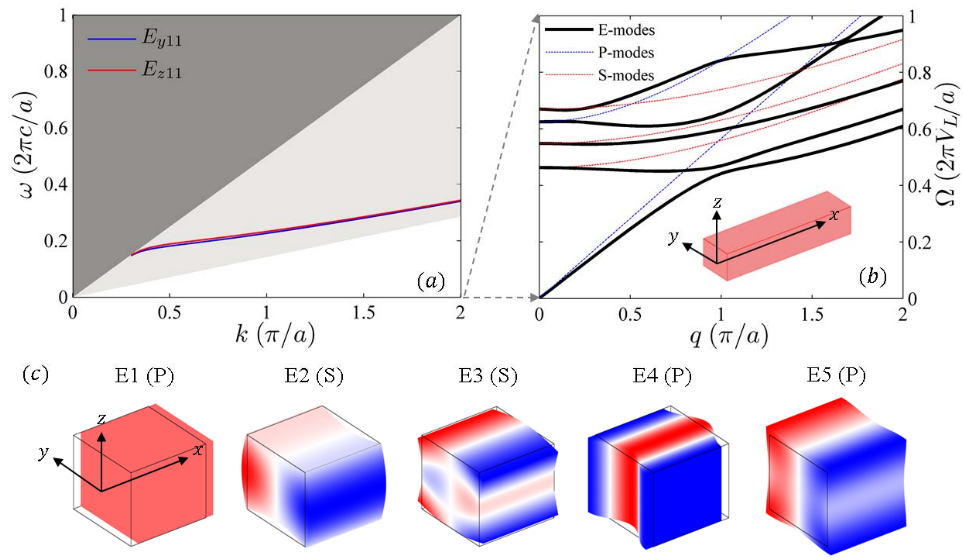

Fig. 1. The guided optical and elastic modes of a silicon rectangular waveguide. Optical frequency is in unit of $2\pi c/a$, while elastic frequency is in unit of $2\pi V_L/a$. $V_L = \sqrt{E/\rho} = 8.54 \times 10^3$m/s is the velocity of longitudinal elastic waves in bulk silicon. (a) Dispersion relation of optical modes E_{y11} and E_{z11}. (b) Dispersion relation of elastic modes which have even symmetry with respect to both $y = 0$ and $z = 0$ planes. E-modes (black lines) are the eigen-modes of the actual silicon waveguide, with silicon-air interfaces treated as free boundaries. For comparison, the dispersion relations of purely longitudinal modes (designated as P-modes, blue curves) and purely transverse modes (designated as S-modes, red curves) are included. They are constrained respectively with x-only displacement, and y-z-only movements. At $q = 0$, E-modes manifest as either P-modes or S-modes. (c) The displacement profiles of mode E1 through E5 at $q = 0$, with the peak deformation shown. The color represents y-displacement (u_y) for S-like E modes and x-displacement(u_x) for P-like E modes. Blue, white, and red correspond to negative, zero, and positive values respectively. Mode E1 experience a DC longitudinal offset at $\Omega = 0$.

#197459 - $15.00 USD Received 12 Sep 2013; revised 18 Nov 2013; accepted 18 Nov 2013; published 12 Dec 2013

$q \neq 0$. At $q = 0$, the mirror reflection symmetry with respect to plane $x = 0$ is conserved . Odd (even) modes with respect to $x = 0$ are purely longitudinal (transverse), separating E-modes into P-modes and S-modes. At nonzero q, silicon-air boundaries hybridize the P-modes and the S-modes, resulting in E-modes with both longitudinal and transverse movement. Similar to the optical mode, we can choose a proper phase so that u_x is imaginary while $u_{y,z}$ are real.

3.1. Forward SBS

Spontaneous forward -Brillouin light scattering (i.e. or scattering from thermally populated phonons) was first observed in optical fiber in 1985 [56, 57]. However, in conventional optical fibers forward stimulated Brillouin scattering (forward-SBS) processes are exceedingly weak (typically orders of magnitude weaker than backward SBS). This is due to poor confinement (or delocalization) of the slow-group velocity phonon modes that mediate photon-phonon coupling in the forward scattering geometry [4, 27, 31]. However, waveguides with nanoscale feature sizes can efficiently produce FSBS, for example, in photonic crystal fibers [4] and suspended silicon waveguides [31]. The frequency of the excitable elastic modes in FSBS is pinned by the structure, independent of the incident optical frequency. Both structures provide strong transverse phonon confinement, and such optical-phonon-like elastic modes are automatically phase-matched to higher orders of Stokes and anti-Stokes optical waves. The cascaded generation of such elastic modes through an optical frequency can enable efficient phonon generation with large quantum efficiency [4].

In FSBS, $\mathbf{E}_p = \mathbf{E}_s = \mathbf{E}$ and $q = 0$. Equation (14) can be simplified to

$$\begin{bmatrix} \sigma_{xx} \\ \sigma_{yy} \\ \sigma_{zz} \\ \sigma_{yz} \\ \sigma_{xz} \\ \sigma_{xy} \end{bmatrix} = -\frac{1}{2}\varepsilon_0 n^4 \begin{bmatrix} p_{11} & p_{12} & p_{13} & & & \\ p_{12} & p_{22} & p_{23} & & & \\ p_{13} & p_{23} & p_{33} & & & \\ & & & p_{44} & & \\ & & & & p_{55} & \\ & & & & & p_{66} \end{bmatrix} \begin{bmatrix} |E_x|^2 \\ |E_y|^2 \\ |E_z|^2 \\ 2Re(E_y E_z^*) \\ 0 \\ 0 \end{bmatrix}. \tag{23}$$

Apparently, $\sigma_{xy} = \sigma_{xz} = 0$. From Eqs. (15) and (16), we conclude that $f_x^{ES} = F_x^{ES} = 0$. So both electrostriction force and radiation pressure in FSBS are transverse. We pick an operating point at $\omega = 0.203(2\pi c/a)$, $k = 0.75(\pi/a)$ with $a = 315$nm, and compute the force distribution (Fig. 2(a)). Electrostriction body force is largely in the y direction, because E_y is the dominant component in electric field and $|p_{11}|$ is about five times larger than $|p_{12}|$. Electrostriction pressure points inwards, where radiation pressure points outwards. Radiation pressure is about five times greater than electrostriction pressure. The transverse nature of optical force combined with the fact that elastic modes are either P-modes or S-modes at $q = 0$ indicates that only S-modes have nonzero FSBS gains. The corresponding FSBS gains are calculated using a mechanical quality factor of $Q = 1000$ for all the elastic modes (Fig. 2(b)). As expected, only S-modes E2, E3, and E5 have nonzero gains. Mode E2 has the largest gain of $1.72 \times 10^4 \mathrm{m}^{-1}\mathrm{W}^{-1}$, which comes from a constructive combination of electrostriction ($0.42 \times 10^4 \mathrm{m}^{-1}\mathrm{W}^{-1}$) and radiation pressure ($0.44 \times 10^4 \mathrm{m}^{-1}\mathrm{W}^{-1}$). Mode E5 has a total gain of $0.51 \times 10^4 \mathrm{m}^{-1}\mathrm{W}^{-1}$, which mainly comes from radiation pressure ($0.36 \times 10^4 \mathrm{m}^{-1}\mathrm{W}^{-1}$).

To illustrate the interplay between electrostriction and radiation pressure, we scale the waveguide dimension a from 250nm to 2.5μm by raising the operating point in the optical dispersion diagram from $0.16(2\pi c/a)$ to $1.61(2\pi c/a)$, and compute the corresponding FSBS gains for mode E2 and E5 (Fig. 2(c)). For both E2 and E5, the FSBS gain from electrostriction scales as $1/a^2$ for large a. This can be understood by a detailed analysis of Eq. (10). Under normalization condition $\langle \mathbf{E}, \varepsilon\mathbf{E} \rangle = 1$, the electrostriction tensor scales as $1/a^2$. Since electrostriction force is

#197459 - $15.00 USD Received 12 Sep 2013; revised 18 Nov 2013; accepted 18 Nov 2013; published 12 Dec 2013

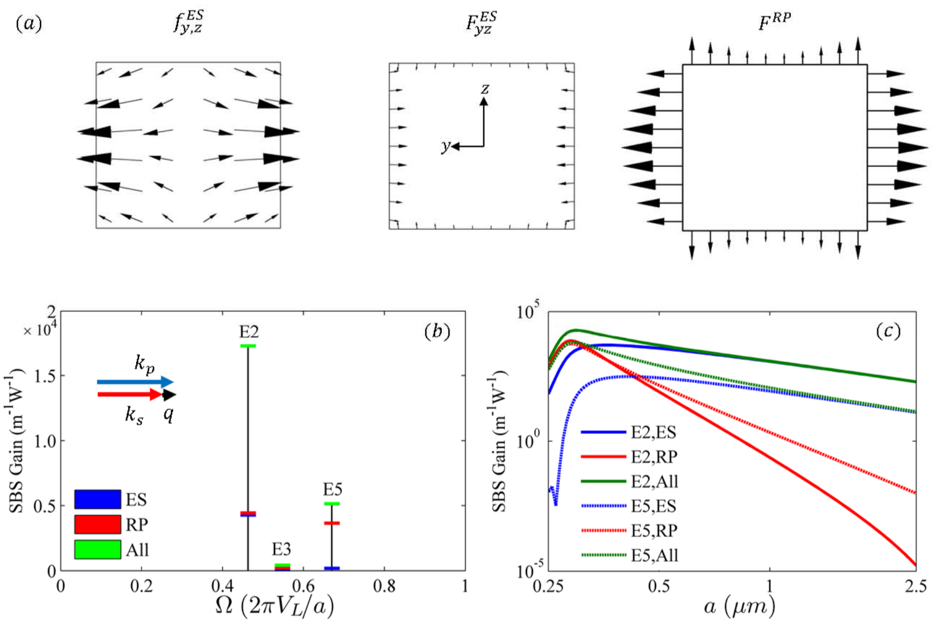

Fig. 2. Optical force distributions and the resultant gain coefficients of the Forward SBS. In panels (a) and (b), the width of the waveguide is $a = 315$nm, and the incident optical waves have $\omega = 0.203(2\pi c/a)$, and $k = 0.75(\pi/a)$. The elastic waves are generated at $q = 0$. (a) The force distribution of electrostriction body force density, electrostriction surface pressure, and radiation pressure respectively. All three types of optical forces are transverse. (b) Calculated FSBS gains of the elastic modes, assuming mechanical $Q = 1000$. Blue, red, and green bars represent FSBS gains under three conditions: electrostriction-only, radiation-pressure-only, and the combined effects. Only the S-like E modes have non-zero gains. (c) The scaling relation of FSBS gains as the device dimension a is varied from 0.25μm to 2.5μm. Solid and dotted curves correspond to the gain coefficients for mode E2 and E5 respectively.

#197459 - $15.00 USD Received 12 Sep 2013; revised 18 Nov 2013; accepted 18 Nov 2013; published 12 Dec 2013

essentially the divergence of electrostriction tensor, the total electrostriction force that apply to the right half of the waveguide scales as $1/a^3$. Under normalization condition $\langle \mathbf{u}_m, \rho \mathbf{u}_m \rangle = 1$, $\mathbf{u}_m$ scales as $1/a$. So the overlap integral scales as $1/a^2$. Under a fixed quality factor, the FSBS gain from electrostriction scales as $1/a^2$.

Unlike the electrostriction contributions that run parallel in different modes, the FSBS gain from radiation pressure scales as $1/a^6$ for mode E5 and $1/a^8$ for mode E2. This can also be understood from a breakdown of Eq. (10). Given the input power, the sum of average radiation pressure on the horizontal and vertical boundaries of the rectangular waveguide is proportional to $(n_g - n_p)/A$, where n_g (n_p) is the group (phase) index, and A is the waveguide cross-section [47]. When the waveguide scales up, $n_g - n_p$ shrinks as $1/A$. As a result, the sum of average radiation pressure scales as $1/a^4$, and the FSBS gain from radiation pressure should scale as $1/a^6$. For mode E2, however, radiation pressures on the horizontal and vertical boundaries generate overlap integrals with opposite signs. It is the difference rather than the sum between the horizontal and vertical radiation pressures that determines the scaling of the FSBS gains from radiation pressure. A closer examination reveals that although the overlap integral from radiation pressure on the horizontal/vertical boundaries scales as $1/a^4$, the net overlap integral from radiation pressure scales as $1/a^5$, resulting in the $1/a^8$ scaling of FSBS gain from radiation pressure for mode E2.

3.2. Backward SBS

In traditional optical fibers, BSBS process is the qualitatively different from FSBS, as it is the only configuration that allows strong photon-phonon coupling. Recent studies have demonstrated on-chip BSBS on chalcogenide rib waveguide [5]. Chip-based BSBS process has been applied in tunable slow light [58], tunable microwave photonic filter [59], and stimulated Brillouin lasers [60].

In BSBS, $\mathbf{E}_p = \mathbf{E}$, $\mathbf{E}_s = \mathbf{E}^*$, and $q = 2k$. Equation (14) can be simplified to

$$\begin{bmatrix} \sigma_{xx} \\ \sigma_{yy} \\ \sigma_{zz} \\ \sigma_{yz} \\ \sigma_{xz} \\ \sigma_{xy} \end{bmatrix} = -\frac{1}{2}\varepsilon_0 n^4 \begin{bmatrix} p_{11} & p_{12} & p_{13} & & & \\ p_{12} & p_{22} & p_{23} & & & \\ p_{13} & p_{23} & p_{33} & & & \\ & & & p_{44} & & \\ & & & & p_{55} & \\ & & & & & p_{66} \end{bmatrix} \begin{bmatrix} E_x^2 \\ E_y^2 \\ E_z^2 \\ 2E_yE_z \\ 2E_xE_z \\ 2E_xE_y \end{bmatrix}. \tag{24}$$

All components of σ_{ij} are nonzero, generating electrostriction force with both longitudinal and transverse components. We pick an operating point at $\omega = 0.203(2\pi c/a)$, $k = 0.75(\pi/a)$ with $a = 315$nm, and compute the force distribution (Fig. 3(a)). Electrostriction body force has large longitudinal component over the waveguide cross-section, which mainly comes from the $-iq\sigma_{xx}$ term in Eq. (15). The hybrid nature of optical forces combined with the fact that all elastic modes are hybrid at nonzero q indicates that all elastic modes have nonzero BSBS gains. We compute the corresponding BSBS gains using a quality factor $Q = 1000$ for all the elastic modes (Fig. 3(b)). For mode E1 and E2, electrostriction force and radiation pressure add up destructively, resulting in small BSBS gains of 0.089×10^4m^{-1}W^{-1} and 0.086×10^4m^{-1}W^{-1} respectively.

Next, we vary a from 250nm to 2.5μm and compute the corresponding BSBS gains for mode E1 (Fig. 3(c)). For comparison, we also compute the conventional BSBS gain G_0. The BSBS gain from electrostriction of mode E1 decays very quickly. In contrast, G_0 scales as $1/a^2$ as required by Eq. (22). The reason is that, although mode E1 starts as a longitudinal plane wave for $q \approx 0$, it quickly evolves into surface-vibrating wave as q increases. There are two ways to recover the scaling of G_0. First, we can force purely longitudinal movement by consider-

#197459 - $15.00 USD Received 12 Sep 2013; revised 18 Nov 2013; accepted 18 Nov 2013; published 12 Dec 2013

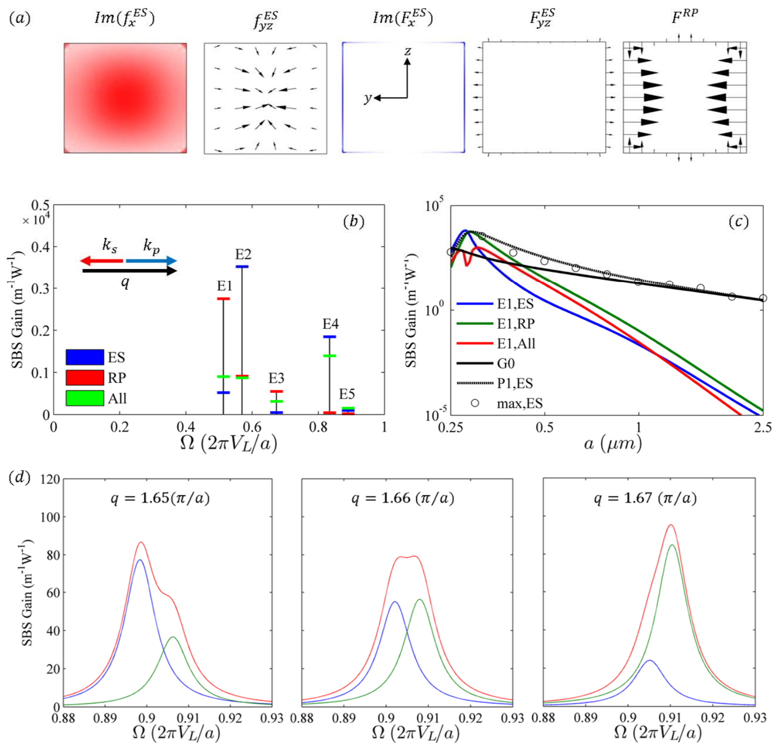

Fig. 3. Optical force distributions and the resultant gain coefficients of the Backward SBS. In panels (a) and (b), the width of the waveguide is $a = 315$nm, and the incident optical waves have $\omega = 0.203(2\pi c/a)$, and $k = 0.75(\pi/a)$. The elastic waves are generated at $q = 1.5(\pi/a)$. (a) The force distribution of electrostriction body force density, electrostriction surface pressure, and radiation pressure respectively. Electrostriction have both longitudinal and transverse components. Radiation pressure are purely transverse. (b) Calculated BSBS gains of the elastic modes, assuming mechanical $Q = 1000$. Blue, red, and green bars represent FSBS gains under three conditions: electrostriction-only, radiation-pressure-only, and the combined effects.(c) The scaling relation of BSBS gains related to mode E1 as a is varied from 0.25μm to 2.5μm, color-coded similar to panel (b). For comparison, gain coefficients predicted by conventional fiber BSBS theory are shown as the solid black curve. The dotted black curve represents the electrostriction-only BSBS gain of the constrained mode P1. Black circles represent the largest electrostriction-only BSBS gain coefficient among all E-modes for a given a. (d) BSBS spectra near the anti-crossing between mode E4 and E5 around $q = 1.66(\pi/a)$. The mechanical quality factor Q is assumed to be 100. The red lines represent the total BSBS gain. The blue and green lines represent contributions from mode E4 and E5.

#197459 - $15.00 USD Received 12 Sep 2013; revised 18 Nov 2013; accepted 18 Nov 2013; published 12 Dec 2013

ing P-modes in Fig. 1(b). Mode P1, the fundamental P-mode, is exactly the longitudinal plane wave, characterized by uniform longitudinal vibrations across the waveguide cross-section and an approximately linear dispersion relation. The BSBS from electrostriction for mode P1 does converge to G_0 (Fig. 3(c)). Second, the dispersion curve of mode P1 intersects with the dispersion curves of many E-modes as q increases. For a given q, the E-modes which are close to the intersection point become P1-like with approximately uniform longitudinal vibrations across the waveguide cross-section. The BSBS gain of these E-modes should be much larger than other E-modes, and close to the gain of mode P1. To verify this point, we compute the BSBS gains of a large number of E-modes. The maximal gain from electrostriction among all the E-modes does converge to G_0 as a exceeds several microns (Fig. 3(c)).

In BSBS, the operating point in the elastic dispersion diagram can be tuned by varying the operating point in the optical dispersion diagram through phase-matching condition $q = 2k$. One unique feature about the elastic dispersion diagram is the abundance of anti-cross between the hybridized elastic modes. The two elastic modes involved in an anti-crossing point typically have disparate spatial distributions and quite different BSBS gains. These two modes will exchange their spatial distributions and corresponding BSBS gains when q is scanned through the anti-cross region, as demonstrated in Fig. 3(d). Figure 3(d) also show that the total gain spectrum can have complex shapes. The frequency response method in [31] can only calculate the aggregated gain. The eigen-mode method developed here can not only separate the contributions from different elastic modes, but also parameterize the gain of individual modes with simple physical quantities.

4. Silicon rectangular waveguide: inter-modal coupling

In this section, we explore inter-modal coupling of the same silicon rectangular waveguide [30]. In inter-modal SBS, pump and Stokes waves can have distinct spatial distributions, which essentially double the degree of freedoms of tailoring optical force distributions. In addition, pump and Stokes waves can have different or even orthogonal polarizations so that the two waves can be easily separated with a polarizing beam splitter. For the rectangular waveguide discussed above, the optical force in intra-modal coupling is always symmetric with respect to $y = 0$ and $z = 0$, exciting elastic modes with the matching symmetry. In inter-modal coupling, however, optical forces with all possible symmetries can be generated, and elastic modes with all possible symmetries can be excited. For instance, we consider the coupling between E_{y11} (pump) and E_{z11} (Stokes). The operating point is $\omega = 0.203(2\pi c/a)$, $k_p = 0.750(\pi/a)$, $k_s = 0.665(\pi/a)$, and $q = 0.085(\pi/a)$ with $a = 315$nm. Because E_{y11} and E_{z11} have the opposite symmetries with respect to both $y = 0$ and $z = 0$, the induced optical force is anti-symmetric with respect to both planes (Fig. 4(a)). Both electrostriction body force and radiation pressure try to pull the waveguide in one diagonal and squeeze the waveguide in the other diagonal. Electrostriction pressure has the opposite effect, but is much weaker than the radiation pressure.

Under such optical force, elastic modes which are odd with respect to both $y = 0$ and $z = 0$ (O-modes) are excited. We calculate the SBS gains of mode O1 through O5 using a mechanical quality factor $Q = 1000$ for all the modes (Fig. 4(b)). Mode O1 represents a rotation around x axis. The overlap integral is proportional to the torque. The y component and z component of the optical forces generate torques with opposite signs, which significantly reduces the total overlap integral. Mode O1 still has a sizable SBS gains because of its small elastic frequency $\Omega = 0.024(2\pi V_L/a)$. Mode O2 represents a breathing motion along the diagonal. Its modal profile coincides quite well with the optical force distribution. The constructive combination between electrostriction force and radiation pressure results in large gain of $1.54 \times 10^4 \text{m}^{-1}\text{W}^{-1}$. Mode O3 only have small SBS gains since it is dominantly longitudinal while the optical forces are largely transverse. The SBS gains of O4, O5 and higher order modes are close to zero

#197459 - $15.00 USD Received 12 Sep 2013; revised 18 Nov 2013; accepted 18 Nov 2013; published 12 Dec 2013

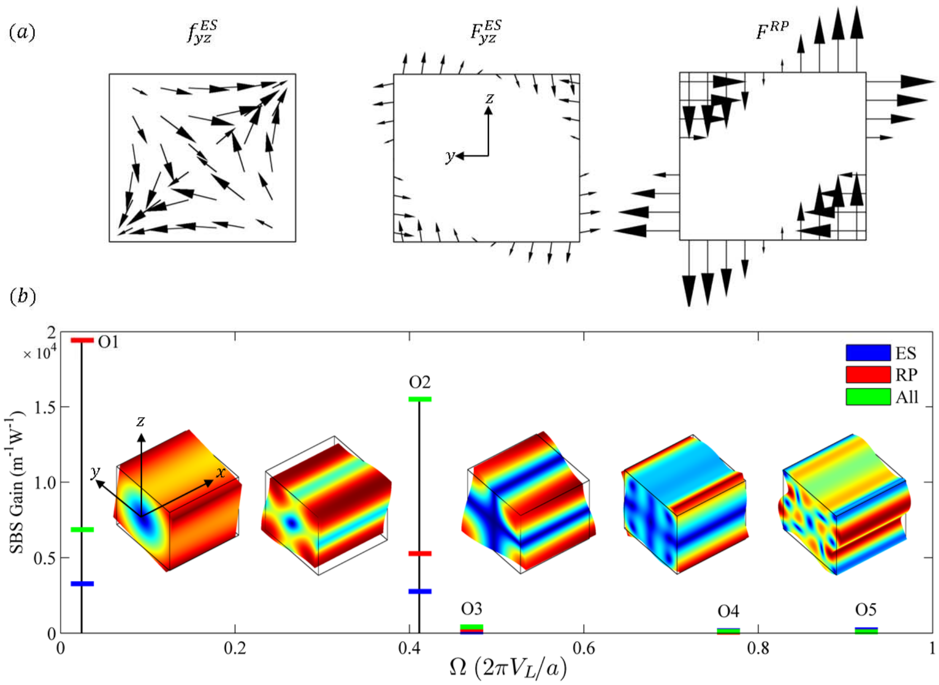

Fig. 4. Optical force distributions, relavant elastic modes, and the resultant gain coefficients of inter-modal FSBS between E_{y11} (pump) and E_{z11} (Stokes). The width of the waveguide is set to be $a = 315$nm. The incident optical waves have $\omega = 0.203(2\pi c/a)$, with the pump-wave propagation constant at $k_p = 0.750(\pi/a)$, and the Stokes-wave propagation constant at $k_s = 0.665(\pi/a)$. The elastic waves are generated at $q = 0.085(\pi/a)$. (a) The force distribution of electrostriction body force density, electrostriction surface pressure, and radiation pressure respectively. The longitudinal forces (not shown here) are negligible, in comparison to the transverse forces. All optical forces are anti-symmetric with respect to plane $y = 0$ and plane $z = 0$, exciting elastic modes with the matching symmetry (designated as O-modes). (b) Calculated inter-modal SBS gains, assuming mechanical $Q = 1000$. The insets illustrate the displacement profiles of mode O1 through O5 at $q = 0.085(\pi/a)$, at peak deformation. "Jet" color map is used to shown the amplitude of *total* displacement. Blue and red correspond to zero and maximum respectively.

#197459 - $15.00 USD Received 12 Sep 2013; revised 18 Nov 2013; accepted 18 Nov 2013; published 12 Dec 2013

mainly because the complicated mode profiles is spatially mismatched with the optical force distribution: the rapid spatial oscillation of the elastic modes cancels out the overlap integrals to a large extent.

5. Concluding remarks

In this article, we present a general framework of calculating the SBS gain via the overlap integral between optical forces and elastic eigen-modes. Our method improved upon the frequency response representation of SBS gains [31]. By decomposing the frequency response into elastic eigen-modes, we show that the SBS gain is the sum of many Lorentzian components which center at elastic eigen-frequencies. The SBS gain spectrum is completely determined by the quality factor and maximal gain of individual elastic modes. Therefore, our method is conceptually clearer and computationally more efficient than the frequency response method. Through the study of a silicon waveguide, we demonstrate that our method can be applied to both FSBS and BSBS, both intra-modal and inter-modal coupling, both nanoscale and microscale waveguides. Both analytical expressions and numerical examples show that SBS nonlinearity is tightly connected to the symmetry, polarization, and spatial distributions of optical and elastic modes. The overlap integral formula of SBS gains provides the guidelines of tailoring and optimizing SBS nonlinearity through material selection and structural design.

Acknowledgments

The authors acknowledge support from the MesoDynamic Architectures program at the DARPA under the direction of Dr Jeffrey L. Rogers. Z.W acknowledges support from the Alfred. P. Sloan Research Fellowship. We are grateful to Whitney Purvis Rakich for careful reading and critique of this manuscript.

#197459 - $15.00 USD Received 12 Sep 2013; revised 18 Nov 2013; accepted 18 Nov 2013; published 12 Dec 2013